

# Observation of Electric-Dipole Transitions in the Laser-Cooling Candidate $\text{Th}^-$

Rulin Tang,<sup>1,\*</sup> Ran Si,<sup>2,3,\*</sup> Zejie Fei,<sup>4</sup> Xiaoxi Fu,<sup>1</sup> Yuzhu Lu,<sup>1</sup> Tomas Brage,<sup>2,3</sup> Hongtao Liu,<sup>4,†</sup> Chongyang Chen,<sup>3,‡</sup> and Chuangang Ning<sup>1,5,§</sup>

<sup>1</sup>*Department of Physics, State Key Laboratory of Low-Dimensional Quantum Physics, Tsinghua University, Beijing 100084, China*

<sup>2</sup>*Division of Mathematical Physics, Department of Physics, Lund University, P.O. Box 118, 221 00 Lund, Sweden*

<sup>3</sup>*Shanghai EBIT Lab, Key Laboratory of Nuclear Physics and Ion-beam Application (MOE), Institute of Modern Physics, Department of Nuclear Science and Technology, Fudan University, Shanghai 200433, China*

<sup>4</sup>*Key Laboratory of Interfacial Physics and Technology, Shanghai Institute of Applied Physics, Chinese Academy of Sciences, Shanghai 201800, China*

<sup>5</sup>*Collaborative Innovation Center of Quantum Matter, Beijing 100084, China*

(Dated: November 15, 2019)

## Abstract

Despite the fact that the laser cooling method is a well-established technique to obtain ultra-cold neutral atoms and atomic cations, it has so far never been applied to atomic anions due to the lack of suitable electric-dipole transitions. Efforts of more than a decade currently have  $\text{La}^-$  as the only promising candidate for laser cooling. Our previous work [Tang et al., Phys. Rev. Lett. 123, 203002(2019)] showed that  $\text{Th}^-$  is also a potential candidate. Here we report on a combination of experimental and theoretical studies to determine the relevant transition frequencies, transition rates, and branching ratios in  $\text{Th}^-$ . The resonant frequency of the laser cooling transition is determined to be  $\nu/c = 4118.0(10) \text{ cm}^{-1}$ . The transition rate is calculated as  $A = 1.17 \times 10^4 \text{ s}^{-1}$ . The branching fraction to dark states is very small,  $1.47 \times 10^{-10}$ , thus this represents an ideal closed cycle for laser cooling. Since Th has zero nuclear spin, it is an excellent candidate to be used to sympathetically cool antiprotons in a Penning trap.

The achievement of Bose-Einstein condensation, precision spectroscopy, and tests of fundamental symmetries has opened a new chapter in atomic and molecular physics. The main driving force behind this achievement is the ability to cool atoms and positive ions to  $\mu\text{K}$  or even lower temperatures via laser cooling techniques. Although laser cooling is a well-established technique for producing ultra-cold neutral atoms and positive ions, it has not yet been achieved for negative ions. In principle, once we produce ultracold ensembles of a specific anion system, we can use them to sympathetically cool any anions, ranging from elementary particles to molecular anions, which will promote the research of cold plasma[1], ultracold chemistry[2], and fundamental-physics tests[3–8]. In contrast to neutral atoms and positive ions, which have an infinite number of bound states, negative ions have only a single bound state in most cases. The reason is that in atomic anions, the excess electron is bound mainly via polarization and correlation effects[9]. The potential experienced by this extra electron is shallow and of short range, and can therefore usually not possess bound excited states[9, 10]. There are a few exceptions to this rule with atomic anions having bound excited states. It is even more rare that these bound states are of opposite parity[9, 11], which can give rise to electric dipole ( $E1$ ) transitions. As a matter of fact, there are so far only three reported  $E1$  observations in atomic anions, for  $\text{Os}^-$ [11–15],  $\text{Ce}^-$ [16, 17], and  $\text{La}^-$ [11, 18–20], where only  $\text{La}^-$  is a promising candidate for laser cooling[20]. The frequency and rate of the laser cooling transition was determined to be  $\nu = 96.592\,713(91)$  THz[19, 20] and  $A = 4.90(50) \times 10^4 \text{ s}^{-1}$ [20], respectively. There are two major obstacles in using  $\text{La}^-$  for cooling. Firstly, the dark states involved in the cooling transition cycle  ${}^3F_2^e \leftrightarrow {}^3D_1^o$  give a population of metastable states. As an example, during the period of laser cooling an ensemble of  $\text{La}^-$  ions from 100 K to Doppler temperature  $T_D = 0.17 \mu\text{K}$ , roughly 40% of  $\text{La}^-$  will end up in the metastable state  ${}^3F_3^e$  with a lifetime of 132 s[20]. Secondly, the nuclear spin of  ${}^{139}\text{La}^-$  is  $7/2$ , resulting in five hyperfine structure levels within the ground state  ${}^3F_2^e$  of  ${}^{139}\text{La}^-$  (with  $F = 11/2, 9/2, 7/2, 5/2, 3/2$ ), three for the excited state  ${}^3D_1^o$  (with  $F = 9/2, 7/2, 5/2$ ), and seven for the metastable state  ${}^3F_3^e$  (with  $F = 13/2, 11/2, 9/2, 7/2, 5/2, 3/2, 1/2$ ). Since several hyperfine levels involved in the cooling cycle are dark states, repumping laser beams are required to close the transition cycle[19].

Recently, we pointed out that  $\text{Th}^-$  is also a potential candidate for laser cooling based on results from high-resolution photoelectron energy spectroscopy and highly accurate theoretical calculations[21]. The electron affinity (EA) of  $\text{Th}^-$  was determined to be

4901.35(48)  $\text{cm}^{-1}$  or 0.607 690(60) eV. The transition for laser cooling was identified as  ${}^4F_{3/2}^e \leftrightarrow {}^2S_{1/2}^o$  in  $\text{Th}^-$  with a transition energy of  $3904 \text{ cm}^{-1}$ , and a relatively fast transition rate of  $A = 1.17 \times 10^4 \text{ s}^{-1}$ . Since the Th isotope 232 has zero nuclear spin and therefore no hyperfine structure, it introduces much less potential complications for laser-cooling than  $\text{La}^-$ . This advantage is emphasized for sympathetically cooling antiprotons via laser-cooled anions. Both  $\text{La}^-$  and the molecular anion  $\text{C}_2^-$  have been proposed as two candidates[5, 13, 22], but in the roadmap towards producing cold antihydrogens, the decelerated antiprotons are trapped and precooled in a Penning trap[7, 8], where a strong magnetic field of a few Tesla is used to confine antiprotons. The simpler structure of energy levels of  $\text{Th}^-$  makes it possible to be laser cooled in this kind of traps. In a magnetic field, the ground state  ${}^4F_{3/2}^e$  and the excited state  ${}^2S_{1/2}^o$  are split up into four and two sublevels, respectively, due to the Zeeman effects. This is in sharp contrast to the hyperfine affected system of  $\text{La}^-$ , which will become very complex in a magnetic field. The challenge of laser-cooling molecular anions, such as  $\text{C}_2^-$ , is to recycle vibrational and rotational branchings of the cooling transition[5, 22]. Obviously, the laser cooling of  $\text{Th}^-$  in a Penning trap is more attractive than in a Paul trap because the precooled antiproton can be transferred and trapped efficiently using the same magnetic field.

In this letter, we report the experimental observation of the bound-bound electrical dipole transitions in  $\text{Th}^-$  from the ground state  ${}^4F_{3/2}^e$  to excited states  ${}^2S_{1/2}^o$ ,  ${}^4F_{5/2}^o$ , and  ${}^4D_{1/2}^o$  by the resonant two-photon detachment method. We experimentally determine the resonance frequencies and obtain two-photon detachment photoelectron spectra at the resonant frequencies. Based on the previous theoretical calculations, we further extend the search for all possible bound states of  $\text{Th}^-$ . Moreover, to address the question of to which degree the cooling cycle is closed, all relevant branching ratios of transitions are deduced.

The experiment is conducted using our cryogenic slow electron velocity-mapping imaging (cryo-SEVI) spectrometer[23–25], which is described in detail in earlier publications[26]. The slow electron velocity-mapping imaging (SEVI) method has a high energy resolution for low-kinetic-energy electrons. We have used this method to determine the electron affinity (EA) of several transition elements[27–29], such as Re[30], Hf[31] and La[32].  $\text{Th}^-$  ions are produced by laser sputtering on a pure thorium metal disk. Generated anions lose their kinetic energy via collisions with the buffer gas and are trapped in a radio-frequency (RF) octupole ion trap, which is mounted on a cryogenically cold head with a controlled temperature in the

rang 5–300 K. In this experiment, the mixture of 20% H<sub>2</sub> and 80% He is used as buffer gas, which is delivered by a pulsed valve. Th<sup>-</sup> anions are stored in the trap for a period of 45 ms, and the temperature is kept at 300 K. Under the experimental conditions, our experimental results show that all excited Th<sup>-</sup> decay to the ground state. The trapped anions are then extracted via pulsed potentials on the end caps of the ion trap and analyzed by a Wiley-McLaren type time-of-flight (TOF) mass spectrometry[33]. Using a mass gate, we can select Th<sup>-</sup> anions via a setting of  $m = 232$ . Next, a probing laser beam with an adjustable wavelength intersects the ion beam orthogonally and photodetaches Th<sup>-</sup>. The emitted electrons form a spherical shell and are projected onto a phosphor screen by the electric field of the velocity-map imaging system[34]. Each bright spot fired by a photoelectron on the phosphor screen is measured and its position is recorded with an event-counting mode via a CCD camera. Since the probing laser beam is linearly polarized parallel to the phosphor screen, the distribution of photoelectrons has cylindrical symmetry. Hence, the 3D photoelectron spherical shell can be reconstructed from the projected 2D distribution without losing information. We use the maximum-entropy reconstruction method[35] to reconstruct the distribution of photoelectrons. The corresponding binding energy (BE) of the detachment channel is extracted from  $BE = h\nu - \alpha r^2$ , where  $h\nu$  is the photon energy,  $r$  is the radius of the spherical shell, and  $\alpha$  is a calibration coefficient, which can be determined by changing  $h\nu$ .

To observe the  $E1$  transitions in Th<sup>-</sup>, we have recently modified the imaging system of the spectrometer, making it possible to switch from the standard SEVI mode to the scanning mode. In the scanning mode, the phosphor screen is used as a charged particle detector. A high-speed oscilloscope is connected to the phosphor screen to record both the photoelectron signals and the residual Th<sup>-</sup> signals after photodetachment. Due to the smaller mass of the photoelectrons, their arrival time is earlier than that of the Th<sup>-</sup> anions. Therefore, one channel can be used to record both signals. Since the one-color laser is used both for the resonant absorption and the photodetachment, it is possible to survey photon energies from  $EA/2$  to  $EA$ . When the laser frequency is at the resonance, Th<sup>-</sup> anions can absorb one photon and reach an excited state. The excited Th<sup>-</sup> anions will then be detached by absorbing another photon, leading to a signal of photoelectrons. When the laser wavelength goes far from the resonance, two-photon detachment process cannot occur and there is no photoelectron. To take into account the intensity fluctuation of the Th<sup>-</sup> anion beam, the

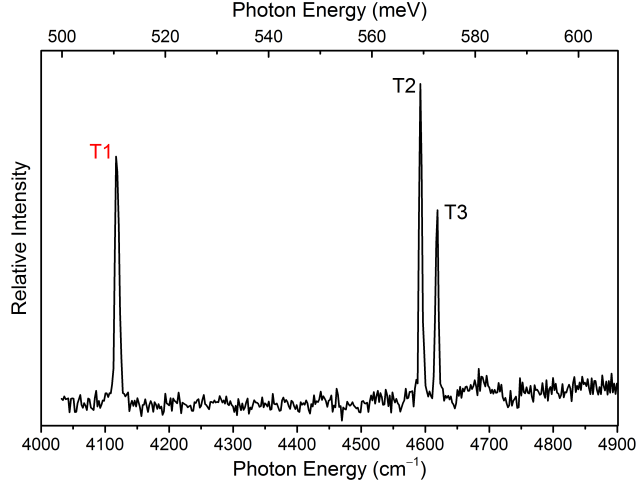


FIG. 1. Survey scan showing three resonances (T1, T2, and T3) in the range from 4050 to 4900  $\text{cm}^{-1}$ .

ratio of the intensity of the photoelectron signal to that of  $\text{Th}^-$  anion beam is plotted versus the scanned wavelength. In both modes, the spectrometer runs at a 20-Hz repetition rate.

To investigate the resonance we use the idle light of an OPO laser (primoScan) pumped by 355 nm, the third harmonic of the Nd:YAG (Quanta-Ray Lab 190). The idle light ranges from 700 to 2700 nm with a linewidth of about  $5 \text{ cm}^{-1}$ . Due to the limitation of the absorption of water vapor in the air and the signal-to-noise ratio, we performed a rough scan ranged from  $4000 \text{ cm}^{-1}$  to  $4900 \text{ cm}^{-1}$  with a step of  $2 \text{ cm}^{-1}$  to obtain an overall spectrum. As shown in Figure 1, three strong resonances were observed, labeled T1, T2, and T3. The full widths at half maximum (FWHM) of peaks are about  $8 \text{ cm}^{-1}$ , mainly due to the broad linewidth of the OPO laser.

To determine the resonant frequency as accurate as possible, we scan the observed resonances with a step size of only  $0.2 \text{ cm}^{-1}$  using the infrared difference frequency generation (DFG) system (Sirah). The infrared laser is produced by a nonlinear DFG effect between a dye laser and a 1064 nm laser. The 1064 nm laser beam is the residual fundamental output of the pump laser. The dye laser is pumped by 532 nm, the second harmonic output of the Nd:YAG (Quanta-Ray Lab 190). Residual 1064 nm laser is mixed with the dye laser in a nonlinear  $\text{LiNbO}_3$  crystal, producing infrared light with a frequency corresponding to the difference between the frequencies of the 1064 nm and the dye laser. The photon energies of the dye laser and the 1064 nm pumping laser are measured by a wavelength meter (HighFinesse

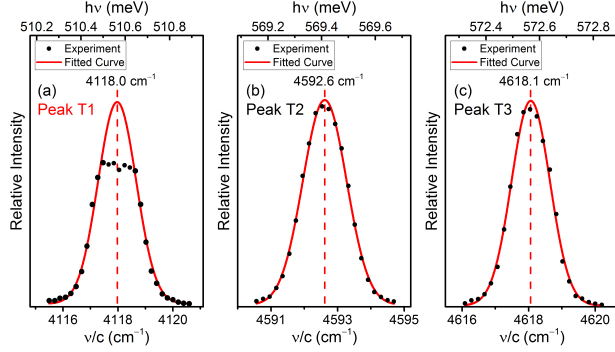


FIG. 2. Fine scans of the three resonances T1, T2, and T3. The solid lines indicated Gaussian fittings. Peak centers, indicated by the dashes lines, are  $4118.0 \text{ cm}^{-1}$ ,  $4592.6 \text{ cm}^{-1}$ , and  $4618.1 \text{ cm}^{-1}$ , respectively. Peak T1 is assigned to the laser cooling transition  ${}^4F_{3/2}^e \leftrightarrow {}^2S_{1/2}^o$ .

WS6-600) with an uncertainty of  $0.02 \text{ cm}^{-1}$ . The linewidth of the dye laser is  $0.06 \text{ cm}^{-1}$ , and  $\sim 1 \text{ cm}^{-1}$  for the unseeded 1064 nm laser, leading to  $\sim 1 \text{ cm}^{-1}$  for the final difference-frequency light. The acquired data of each peak are then fitted to a Gaussian function, as shown in Figure 2. The flat top of peak T1 is due to the saturation of resonance absorption. The resonance energies of T1, T2, and T3 are determined to be  $4118.0 \text{ cm}^{-1}$ ,  $4592.6 \text{ cm}^{-1}$  and  $4618.1 \text{ cm}^{-1}$ , respectively, with FWHMs of  $1.6 \text{ cm}^{-1}$ ,  $1.5 \text{ cm}^{-1}$  and  $1.4 \text{ cm}^{-1}$ , respectively. The widths of the three peaks mainly come from the DFG laser linewidth of about  $1 \text{ cm}^{-1}$  and the power broadening. Other possible contributions, such as Doppler broadening, natural linewidth, are significantly smaller. The uncertainty of the resonance energy is estimated to be  $1.0 \text{ cm}^{-1}$  (30 GHz).

To interpret the experimental results, we extended our calculations using the large-scale multi-configuration Dirac-Hartree-Fock (MCDHF) method[36] as implemented in the GRASP2K package[37]. Compared with our previous calculations[21], we further extend the search for all possible bound states of  $\text{Th}^-$  anion. Three more excited states were found, in the form of  $6d^37s^2 {}^4P_{3/2}^e$ ,  $6d^27s^27p {}^4D_{3/2}^o$ , and  $6d^27s^27p {}^4D_{1/2}^o$ , which are listed along with previous results in Table I. Decay branching fractions and transition rates of the bound states of anions are two key aspects for laser cooling. Table II lists the calculated transition rates[38, 39], absorption line strengths[40], and branching fractions for upper levels lower than and including  ${}^2S_{1/2}^o$  in  $\text{Th}^-$ , including the electric-dipole ( $E1$ ), electric-quadrupole ( $E2$ ), magnetic-dipole ( $M1$ ), and magnetic-quadrupole ( $M2$ ) transitions. Details for the

TABLE I. Measured and calculated excitation energies and lifetimes  $\tau$  of excited states of  $\text{Th}^-$  states.

State	Measured		Calculated		
	$\text{cm}^{-1}$	meV	$\text{cm}^{-1}$	meV	$\tau$
$6d^37s^2\ ^4F_{3/2}^e$			0	0	
$6d^27s^27p\ ^4G_{5/2}^o$			401	50	51.3 ms
$6d^37s^2\ ^4F_{5/2}^e$	1657(6)	205.4(7)	1377	171	0.458 s
$6d^37s^2\ ^4F_{7/2}^e$	2896(10)	359.1(12)	2642	328	8.08 ms
$6d^27s^27p\ ^4F_{3/2}^o$			3033	376	15.9 ms
$6d^37s^2\ ^4F_{9/2}^e$			3637	451	45.6 s
$6d^27s^27p\ ^2S_{1/2}^o$	4118.0(10)	510.57(12)	3904	484	85.5 ms
$6d^27s^27p\ ^4F_{7/2}^o$			3974	493	138 ms
$6d^27s^27p\ ^4F_{5/2}^o$	4618.1(10)	572.57(12)	3992	495	42.4 ms
$6d^37s^2\ ^4P_{3/2}^e$			4284	531	274 ms
$6d^27s^27p\ ^4D_{3/2}^o$			4445	551	180 ms
$6d^27s^27p\ ^4D_{1/2}^o$	4592.6(10)	569.41(12)	4503	558	44.4 ms

calculations of all transitions are summarized in the Supplemental Material[41]. From our results, we can deduce that the possible  $E1$ -allowed transitions in our scanning range are from the ground state  $^4F_{3/2}^e$  to the excited  $^2S_{1/2}^o$ ,  $^4F_{5/2}^o$ ,  $^4D_{3/2}^o$ , and  $^4D_{1/2}^o$ . The line strength for  $^4F_{3/2}^e \rightarrow ^4D_{3/2}^o$  is  $1.98 \times 10^{-2}$ , one order of magnitude smaller than that of the other three transitions. As expected, this transition was not observed in our experiments due to the signal-to-noise limitation.

To further support the identification of the transitions responsible for the observed peaks, we can use additional information provided by the final states of the photodetachment. Figure 3 shows the resonant two-photon detachment photoelectron energy spectra of  $\text{Th}^-$  at the three observed resonant energies, where we use the same labels as in our earlier and consistent one-step detachment experiment[21]. It is clear that the energy spectra acquired at the three resonances are quite different. Using the selection rules of photodetachment[42], it is clear that T1 can be assigned to the laser cooling transition  $^4F_{3/2}^e \rightarrow ^2S_{1/2}^o$  unambiguously. However, at the current stage, it is not possible to make definite identifications for T2 and

TABLE II. Calculated transition energies, line strengths  $S$ , transition rates  $A$ , and branching fraction of transitions except ones with an upper level higher than  ${}^2S_{1/2}^o$  in  $\text{Th}^-$ . Numbers in brackets represent powers of 10. A full list can be found in the Supplemental Material[41].

Upper level	Lower level	$S$ (a.u.) <sup>a</sup>	$A$ (s <sup>-1</sup> )	Branching fraction
${}^4G_{5/2}^o$	${}^4F_{3/2}^e$	8.98[-1]	1.95[+1]	1
${}^4F_{5/2}^e$	${}^4F_{3/2}^e$		1.00[-1]	0.046
	${}^4G_{5/2}^o$	6.63[-3]	2.08[+0]	0.954
${}^4F_{7/2}^e$	${}^4F_{3/2}^e$		1.44[-5]	1.16[-7]
	${}^4G_{5/2}^o$	4.34[-2]	1.24[+2]	0.9994
	${}^4F_{5/2}^e$		7.74[-2]	0.000 625
${}^4F_{3/2}^o$	${}^4F_{3/2}^e$	4.43[0]	6.26[+4]	0.9968
	${}^4G_{5/2}^o$		2.58[-3]	4.10[-8]
	${}^4F_{5/2}^e$	8.72[-2]	2.01[+2]	0.003 195
	${}^4F_{7/2}^e$		1.96[-13]	3.13[-18]
${}^4F_{9/2}^e$	${}^4G_{5/2}^o$		9.62[-9]	4.38[-7]
	${}^4F_{5/2}^e$		2.39[-6]	0.000 11
	${}^4F_{7/2}^e$		2.19[-2]	0.999 89
${}^2S_{1/2}^o$	${}^4F_{3/2}^e$	1.94[-1]	1.17[+4]	0.999 999 98
	${}^4G_{5/2}^o$		1.72[-6]	1.47[-10]
	${}^4F_{5/2}^e$		2.10[-9]	1.80[-13]
	${}^4F_{3/2}^o$		2.32[-4]	1.98[-8]

<sup>a</sup> in atomic unit (a.u.), only electric-dipole ( $E1$ ) transitions were considered.

T3, but a tentative assignment would be  ${}^4F_{3/2}^e \rightarrow {}^4F_{5/2}^o$ , and  ${}^4F_{3/2}^e \rightarrow {}^4D_{1/2}^o$  for T2 and T3, respectively, but it still needs further theoretical confirmation. See the Supplemental Material[41] for the detailed assignment of observed peaks.

Figure 4 illustrates the relevant branchings of the cooling cycle. The weak transitions with branching ratio less than  $10^{-10}$  can of course be neglected. We can see that almost 100% of  $\text{Th}^-$   ${}^2S_{1/2}^o$  decay to the ground state directly, except a ratio of  $1.47 \times 10^{-10}$  of  $\text{Th}^-$



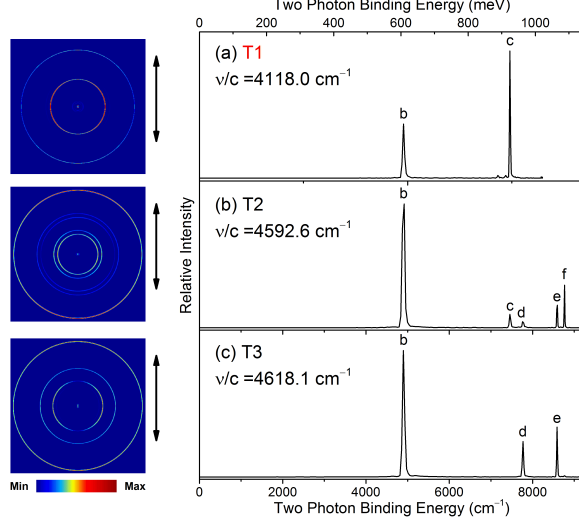


FIG. 3. High-Resolution two-photon photoelectron energy spectra and photoelectron images of  $\text{Th}^-$  at three observed resonances. The double arrow indicates the laser polarization. The peaks labels are consistent with our previous work.

return to the ground state through  ${}^4G_{5/2}^o$ , and  $1.97 \times 10^{-8}$  through  ${}^4F_{3/2}^o$ . The lifetime of  ${}^4F_{3/2}^o$  is  $15.9 \mu\text{s}$ , so  $\text{Th}^-$  anions in  ${}^4F_{3/2}^o$  can quickly decay back to the ground state.  ${}^4G_{5/2}^o$  has a long lifetime of 51.3 ms. Decaying to this long-life metastable state will interrupt the fast transition cycle. Therefore,  ${}^4G_{5/2}^o$  is a dark state from the viewpoint of laser cooling. Fortunately, this branching ratio is very small and clearly negligible. During the period of laser cooling  $\text{Th}^-$  from 10 K to Doppler temperature  $T_D$ , only 0.0004%  $\text{Th}^-$  end up in this state. No repumping laser is required. Therefore, since  $\text{Th}^-$  does not have hyperfine structures, in principle only one laser with a wavelength  $\lambda = 2.4284 \text{ nm}$  is required to realize the laser cooling of  $\text{Th}^-$ . The loss rate due to the photodetachment of the excited  $\text{Th}^-$  during the cooling period is estimated to be a few percent.

In summary, from a combination of experimental and theoretical works we have shown that  $\text{Th}^-$  is an excellent candidate for the laser cooling of anions, where the transition of laser cooling is identified as  ${}^4F_{3/2}^e \leftrightarrow {}^2S_{1/2}^o$ . This cooling cycle is perfectly closed and the branching ended up in a dark state during the cooling period is only  $4 \times 10^{-6}$  relative to the cooling transition. In sharp contrast to  $\text{La}^-$ , the zero nuclear spin of  $\text{Th}^-$  can significantly reduce the cost of the repumping laser system if the laser cooling takes place in a magnetic field. This is an important advantage for sympathetically cooling antiprotons, where a Penning trap is a more practical choice than a Paul trap to co-trap the anions and antiprotons.

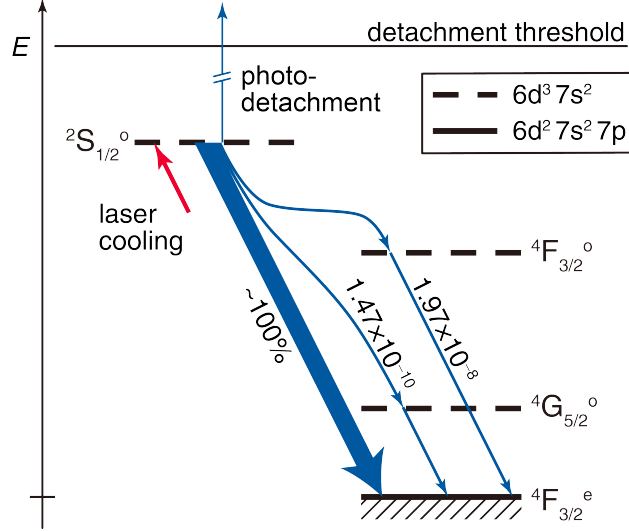


FIG. 4. The decay branches from the  ${}^2S_{1/2}^o$  excited state. The red arrow indicates the pumping direction for laser cooling. Energies are not to scale. Thicknesses of blue arrows are indicative of branching fractions, but not to scale.

Before conducting the laser cooling experiment, a determination of the absolute transition rates, the photodetachment loss, and the resonant frequency of the cooling transition with an accuracy of 10 MHz is required. We will experimentally address this question in the near future.

This work is supported by the National Natural Science Foundation of China (NSFC) (Grants No. 91736102, No. 11974199, No. 21573273, No. 11674066), the National Key R&D Program of China (Grant No. 2018YFA0306504), Strategic Priority Research Program of the Chinese Academy of Sciences (Grant No. XDA02020000). R. S. and T.B. would like to acknowledge support of the Swedish Research Council (VR) under Contract No. 2015-04842. H.T.L would like to acknowledge support of Hundred Talents Program (CAS).

---

\* These authors contribute equally.

† liuhongtao@sinap.ac.cn (HTL)

‡ chychen@fudan.edu.cn (CYC)

§ ningcg@tsinghua.edu.cn (CGN)

[1] T. K. Langin, G. M. Gorman, and T. C. Killian, Laser cooling of ions in a neutral plasma,

- Science **363**, 61 (2019).
- [2] D. S. Jin and J. Ye, Introduction to Ultracold Molecules: New Frontiers in Quantum and Chemical Physics, Chemical Reviews **112**, 4801 (2012).
- [3] M. Amoretti, C. Amsler, G. Bonomi, A. Bouchta, P. Bowe, C. Carraro, C. L. Cesar, M. Charlton, M. Collier, M. Doser, V. Filippini, K. S. Fine, A. Fontana, M. C. Fujiwara, R. Funakoshi, P. Genova, J. S. Hangst, R. S. Hayano, M. H. Holzschneider, L. V. Jorgensen, V. Lagomarsino, R. Landua, D. Lindelof, E. L. Rizzini, M. Macri, N. Madsen, G. Manuzio, M. Marchesotti, P. Montagna, H. Pruys, C. Regenfus, P. Riedler, J. Rochet, A. Rotondi, G. Rouleau, G. Testera, A. Variola, T. L. Watson, and D. P. van der Werf, Production and detection of cold antihydrogen atoms, Nature **419**, 456 (2002).
- [4] M. Ahmadi, B. X. R. Alves, C. J. Baker, W. Bertsche, E. Butler, A. Capra, C. Carruth, C. L. Cesar, M. Charlton, S. Cohen, R. Collister, S. Eriksson, A. Evans, N. Evetts, J. Fajans, T. Friesen, M. C. Fujiwara, D. R. Gill, A. Gutierrez, J. S. Hangst, W. N. Hardy, M. E. Hayden, C. A. Isaac, A. Ishida, M. A. Johnson, S. A. Jones, S. Jonsell, L. Kurchaninov, N. Madsen, M. Mathers, D. Maxwell, J. T. K. McKenna, S. Menary, J. M. Michan, T. Momose, J. J. Munich, P. Nolan, K. Olchanski, A. Olin, P. Pusa, C. Ø. Rasmussen, F. Robicheaux, R. L. Sacramento, M. Sameed, E. Sarid, D. M. Silveira, S. Stracka, G. Stutter, C. So, T. D. Tharp, J. E. Thompson, R. I. Thompson, D. P. van der Werf, and J. S. Wurtele, Observation of the 1S–2S transition in trapped antihydrogen, Nature **541**, 506 (2016).
- [5] S. Gerber, J. Fesel, M. Doser, and D. Comparat, Photodetachment and Doppler laser cooling of anionic molecules, New Journal of Physics **20**, 023024 (2018).
- [6] A. Kellerbauer, M. Amoretti, A. S. Belov, G. Bonomi, I. Boscolo, R. S. Brusa, M. Büchner, V. M. Byakov, L. Cabaret, C. Canali, C. Carraro, F. Castelli, S. Cialdi, M. de Combarieu, D. Comparat, G. Consolati, N. Djourellov, M. Doser, G. Drobychev, A. Dupasquier, G. Ferrari, P. Forget, L. Formaro, A. Gervasini, M. G. Giammarchi, S. N. Gninenko, G. Gribakin, S. D. Hogan, M. Jacquy, V. Lagomarsino, G. Manuzio, S. Mariazzi, V. A. Matveev, J. O. Meier, F. Merkt, P. Nedelec, M. K. Oberthaler, P. Pari, M. Prevedelli, F. Quasso, A. Rotondi, D. Sillou, S. V. Stepanov, H. H. Stroke, G. Testera, G. M. Tino, G. Tréneç, A. Vairo, J. Vigué, H. Walters, U. Warring, S. Zavatarelli, and D. S. Zvezhinskij, Proposed antimatter gravity measurement with an antihydrogen beam, Nuclear Instruments and Methods in Physics Research Section B: Beam Interactions with Materials and Atoms **266**, 351 (2008).

- [7] M. Ahmadi, B. X. R. Alves, C. J. Baker, W. Bertsche, E. Butler, A. Capra, C. Carruth, C. L. Cesar, M. Charlton, S. Cohen, R. Collister, S. Eriksson, A. Evans, N. Evetts, J. Fajans, T. Friesen, M. C. Fujiwara, D. R. Gill, A. Gutierrez, J. S. Hangst, W. N. Hardy, M. E. Hayden, C. A. Isaac, A. Ishida, M. A. Johnson, S. A. Jones, S. Jonsell, L. Kurchaninov, N. Madsen, M. Mathers, D. Maxwell, J. T. K. McKenna, S. Menary, J. M. Michan, T. Momose, J. J. Munich, P. Nolan, K. Olchanski, A. Olin, P. Pusa, C. Ø. Rasmussen, F. Robicheaux, R. L. Sacramento, M. Sameed, E. Sarid, D. M. Silveira, S. Stracka, G. Stutter, C. So, T. D. Tharp, J. E. Thompson, R. I. Thompson, D. P. van der Werf, and J. S. Wurtele, Antihydrogen accumulation for fundamental symmetry tests, *Nature Communications* **8**, 681 (2017).
- [8] M. Doser, C. Amsler, A. Belov, G. Bonomi, P. Bräunig, J. Bremer, R. Brusa, G. Burkhart, L. Cabaret, C. Canali, F. Castelli, K. Chlouba, S. Cialdi, D. Comparat, G. Consolati, L. D. Noto, A. Donzella, A. Dudarev, T. Eisel, R. Ferragut, G. Ferrari, A. Fontana, P. Genova, M. Giammarchi, A. Gligorova, S. Gninenko, S. Haider, J. P. Hansen, S. Hogan, L. Jorgensen, T. Kaltenbacher, A. Kellerbauer, D. Krasnický, V. Lagomarsino, S. Mariazzi, V. Matveev, F. Merkt, F. Moia, G. Nebbia, P. Nedelec, M. Oberthaler, D. Perini, V. Petracek, F. Prezl, M. Prevedelli, C. Regenfus, C. Riccardi, O. Rohne, A. Rotondi, M. Sacerdoti, H. Sandaker, M. Spacek, J. Storey, G. Testera, A. Tokareva, D. Trezzi, R. Vaccarone, F. Villa, Z. Zavatarelli, A. Zenoni, and AEGIS Collaboration, Exploring the WEP with a pulsed cold beam of antihydrogen, *Classical and Quantum Gravity* **29**, 184009 (2012).
- [9] T. Andersen, Atomic negative ions: structure, dynamics and collisions, *Physics Reports* **394**, 157 (2004).
- [10] T. Andersen, H. K. Haugen, and H. Hotop, Binding Energies in Atomic Negative Ions: III, *Journal of Physical and Chemical Reference Data* **28**, 1511 (1999).
- [11] L. Pan and D. R. Beck, Candidates for laser cooling of atomic anions: La<sup>-</sup>-versus Os<sup>-</sup>, *Physical Review A* **82**, 014501 (2010).
- [12] R. C. Bilodeau and H. K. Haugen, Experimental studies of Os<sup>-</sup>: Observation of a bound-bound electric dipole transition in an atomic negative ion, *Physical Review Letters* **85**, 534 (2000).
- [13] A. Kellerbauer and J. Walz, A novel cooling scheme for antiprotons, *New Journal of Physics* **8**, 45 (2006).
- [14] U. Warring, M. Amoretti, C. Canali, A. Fischer, R. Heyne, J. O. Meier, C. Morhard, and A. Kellerbauer, High-Resolution Laser Spectroscopy on the Negative Osmium Ion, *Physical*

- Review Letters **102**, 043001 (2009).
- [15] A. Fischer, C. Canali, U. Warring, A. Kellerbauer, and S. Fritzsche, First Optical Hyperfine Structure Measurement in an Atomic Anion, *Physical Review Letters* **104**, 073004 (2010).
- [16] C. W. Walter, N. D. Gibson, C. M. Janczak, K. A. Starr, A. P. Snedden, R. L. Field III, and P. Andersson, Infrared photodetachment of Ce<sup>-</sup>: Threshold spectroscopy and resonance structure, *Physical Review A* **76**, 052702 (2007).
- [17] C. W. Walter, N. D. Gibson, Y. G. Li, D. J. Matyas, R. M. Alton, S. E. Lou, R. L. Field, D. Hanstorp, L. Pan, and D. R. Beck, Experimental and theoretical study of bound and quasibound states of Ce<sup>-</sup>, *Physical Review A* **84**, 032514 (2011).
- [18] C. W. Walter, N. D. Gibson, D. J. Matyas, C. Crocker, K. A. Dungan, B. R. Matola, and J. Rohlen, Candidate for Laser Cooling of a Negative Ion: Observations of Bound-Bound Transitions in La<sup>-</sup>, *Physical Review Letters* **113**, 063001 (2014).
- [19] E. Jordan, G. Cerchiari, S. Fritzsche, and A. Kellerbauer, High-Resolution Spectroscopy on the Laser-Cooling Candidate La<sup>-</sup>, *Physical Review Letters* **115**, 113001 (2015).
- [20] G. Cerchiari, A. Kellerbauer, M. S. Safronova, U. I. Safronova, and P. Yzombard, Ultracold Anions for High-Precision Antihydrogen Experiments, *Physical Review Letters* **120**, 133205 (2018).
- [21] R. L. Tang, R. Si, Z. Fei, X. X. Fu, Y. Lu, T. Brage, H. Liu, C. Chen, and C. G. Ning, Candidate for Laser Cooling of a Negative Ion: High-Resolution Photoelectron Imaging of Th<sup>-</sup>, *Physical Review Letters* **123**, 749 (2019).
- [22] P. Yzombard, M. Hamamda, S. Gerber, M. Doser, and D. Comparat, Laser Cooling of Molecular Anions, *Physical Review Letters* **114**, 213001 (2015).
- [23] A. Osterwalder, M. J. Nee, J. Zhou, and D. M. Neumark, High resolution photodetachment spectroscopy of negative ions via slow photoelectron imaging, *The Journal of Chemical Physics* **121**, 6317 (2004).
- [24] C. Hock, J. B. Kim, M. L. Weichman, T. I. Yacovitch, and D. M. Neumark, Slow photoelectron velocity-map imaging spectroscopy of cold negative ions, *The Journal of Chemical Physics* **137**, 244201 (2012).
- [25] X. B. Wang and L. S. Wang, Development of a low-temperature photoelectron spectroscopy instrument using an electrospray ion source and a cryogenically controlled ion trap, *Review of Scientific Instruments* **79**, 073108 (2008).

- [26] R. L. Tang, X. X. Fu, and C. G. Ning, Accurate electron affinity of Ti and fine structures of its anions, *The Journal of Chemical Physics* **149**, 134304 (2018).
- [27] X. X. Fu, J. M. Li, Z. H. Luo, X. L. Chen, and C. G. Ning, Precision measurement of electron affinity of Zr and fine structures of its negative ions, *The Journal of Chemical Physics* **147**, 064306 (2017).
- [28] X. L. Chen and C. G. Ning, Accurate electron affinity of Pb and isotope shifts of binding energies of Pb<sup>-</sup>, *The Journal of Chemical Physics* **145**, 084303 (2016).
- [29] Z. H. Luo, X. L. Chen, J. M. Li, and C. G. Ning, Precision measurement of the electron affinity of niobium, *Physical Review A* **93**, 020501(R) (2016).
- [30] X. L. Chen and C. G. Ning, Observation of Rhenium Anion and Electron Affinity of Re, *The Journal of Physical Chemistry Letters* **8**, 2735 (2017).
- [31] R. L. Tang, X. L. Chen, X. X. Fu, H. Wang, and C. G. Ning, Electron affinity of the hafnium atom, *Physical Review A* **98**, 020501(R) (2018).
- [32] Y. Lu, R. L. Tang, X. X. Fu, and C. G. Ning, Measurement of the electron affinity of the lanthanum atom, *Physical Review A* **99**, 062507 (2019).
- [33] W. C. Wiley and I. H. McLaren, Time-of-Flight Mass Spectrometer with Improved Resolution, *Review of Scientific Instruments* **26**, 1150 (1955).
- [34] I. León, Z. Yang, H. T. Liu, and L. S. Wang, The design and construction of a high-resolution velocity-map imaging apparatus for photoelectron spectroscopy studies of size-selected clusters, *Review of Scientific Instruments* **85**, 083106 (2014).
- [35] B. Dick, Inverting ion images without Abel inversion: maximum entropy reconstruction of velocity maps, *Phys. Chem. Chem. Phys.* **16**, 570 (2014).
- [36] C. F. Fischer, M. Godefroid, T. Brage, P. Jönsson, and G. Gaigalas, Advanced multiconfiguration methods for complex atoms: I. Energies and wave functions, *Journal of Physics B: Atomic, Molecular and Optical Physics* **49**, 182004 (2016).
- [37] P. Jönsson, G. Gaigalas, J. Bieroń, C. F. Fischer, and I. P. Grant, New version: Grasp2K relativistic atomic structure package, *Computer Physics Communications* **184**, 2197 (2013).
- [38] F. A. Babushkin, *Acta Physica Polonica* **25**, 749 (1964).
- [39] P. Jönsson, X. He, C. Froese Fischer, and I. P. Grant, The grasp2K relativistic atomic structure package, *Computer Physics Communications* **177**, 597 (2007).
- [40] I. P. Grant, Gauge invariance and relativistic radiative transitions, *Journal of Physics B:*

Atomic and Molecular Physics **7**, 1458 (1974).

- [41] See Supplemental Material at <http://link.aps.org> for details for the calculations of all transitions and detailed assignments of observed peaks.
- [42] P. C. Engelking and W. C. Lineberger, Laser photoelectron spectrometry of Fe-: The electron affinity of iron and the "nonstatistical" fine-structure detachment intensities at 488 nm, Physical Review A **19**, 149 (1979).